Synthesis, structural and thermal characterization of metaphosphatenickel(II) salt

Trilochan Swain

Abstract A new inorganically template metaphosphate of Ni(II) complex has been synthesized and characterized by different measurements such as DSC, FT-IR, C–H–N–S, X-RD and ICP-AES. Differential scanning calorimeter (DSC) elucidated negative specific heat of the system and has used to evaluate some thermodynamical constants like specific heat, enthalpy and entropy of that system. The specific heat capacity of the system is measured in atmospheric O_2 at heating rate of 278 and 283 K min^{-1}. The specific heat is found both positive and negative at 278 K min^{-1}.

Keywords X-RD · DSC · Negative specific heat capacity · Enthalpy · Entropy

Introduction

The preparation and structural chemistry of a number of organically template metal phosphates are extensively studied for their potential applications in many fields in the past few decades [1–6]. Some metal phosphites are reported for replacing metal phosphate [7–10]. The substitution of P(III) for P(V) is observed by Harrison et al. In this case hydrogen phosphate group, $[HPO_3]^{2-}$, which is used as a new basic building block led to diversity of novel structures in organically templated metal phosphates. Many open-framework metal phosphites are synthesized like $[C_2H_{10}N_2]\cdot[V(HPO_3)_2]$, $[C_2H_{10}N_2]\cdot[Fe(HPO_3)_2]$ [11]; $[C_2H_{10}N_2]\cdot[Co_3(HPO_3)_4]$ [12]; $[C_2H_{10}N_2]\cdot[Cr(HPO_3)F_3]$ [13]; $[C_2H_{10}N_2]\cdot[Mn_3(HPO_3)_4]$ [14]. Zhang et al. have been synthesized a new molybdenum(V) nickel phosphate based on divacant $[H_{30}(Mo(V)_{16}O_{32})Ni_{14}(PO_4)_{26}O_2(OH)_4(H_2O)_8]_{12-}$ wheel and structurally characterized [15]. A series of nickel phosphate $(Ni_3(PO_4)_2\cdot 8H_2O)$ three-dimensional (3D) hexahedronal and flower-like architectures were synthesized via a simple template-free hydrothermal route by Wu et al. [16]. Lin et al. have synthesized nanotube arrays of nickel phosphate by electroless deposition into sub-micro to nanometer sized pores of the porous alumina templates by hypophosphite electrolytic solution composed of $NiSO_4$, NaH_2PO_2, $NaC_2H_3O_2$ and $Na_3C_6H_5O_7$ at 80–100 °C and pH 3.6 [17]. Nickel phosphate Versailles Santa Barbara-5 (VSB-5) was synthesized with microwave for 1 h and followed by conventional oven for 2 days in the presence of (2-hydroxyethyl)trimethyl ammonium hydroxide as template by Samadi-Maybodi et al. [18]. Nanoporous nickel phosphates Versailles Santa Barbara-n (VSB-n) attract great interests because their structures are thermostable and include transitional metal [19]. Guillou et al. [20] showed that the open-framework nickel phosphate, VSB-1, is sufficiently stable to be rendered nanoporous and exhibits typical zeolitic properties. However, using only metaphosphoric acid in the preparation of Ni(II) complex is not synthesized till now apart from some organically template complexes. Here, I have evaluated the thermodynamic constants like activation energy, frequency factor, enthalpy, entropy and specific heat capacity of the complex at different heating rates of 278 and 283 K min^{-1}.

In these heating rates specific heat is found negative. The negative specific heat is elucidated by Swain [21, 22]

T. Swain (✉)
Faculty in Chemistry, National Institute of Technology,
Calicut, Kerala, India
e-mail: scienceorissa@rediffmail.com

from metaphosphatecobalt(II) salt and methionine bridged cobalt(III) and copper(II) complex. This negative specific heat is an unusual phenomenon first discovered in statistical models of gravothermal collapse in globular clusters [23]. Motivated further by this fact, the study of specific heat beyond the weak-coupling limit has recently received considerable attention, in particular in view of the validity of the third law of thermodynamics[24–30]. Apart from fundamental thermodynamical questions, the study of specific heat in the quantum regime is also of interest because it can be related to entanglement properties [31]. Recently, two different methods towards the evaluation of a specific heat are proposed and discussed [24]. One possibility based on the thermal expectation value of the Hamiltonian describing the isolated system. Another approach, on which I have focused in this article, is widely used expression for the partition function of the dissipative system [24, 27, 32–39]. It is defined in terms of partition functions of the coupled system and of the uncoupled system.

$$Z = \frac{T_{r_{\mathrm{S+B}}}\mathrm{e}^{-\beta H}}{T_{r_{\mathrm{B}}}\mathrm{e}^{-\beta H_{\mathrm{B}}}} \tag{1}$$

where the total Hamiltonian, $H = H_{\mathrm{S}} + H_{\mathrm{B}} + H_{\mathrm{SB}}$, consisted of contributions from the system, bath and coupling between them. In the absence of coupling between system and bath, Z reduces to the partition function of the system. Partition function (1) appears naturally in the Feynman–Vernon approach to dissipative systems [24] and can be related to the equilibrium properties of the system [40]. I have found the same type of negative specific heat as like metaphosphate cobalt(II) salt by Swain [21, 22].

Experimental

Materials and synthesis

In a typical synthesis for this compound 1 mol of $NiSO_4 \cdot 6H_2O$ and 1 mol of metaphosphoric acid (60% HPO_3 + 40% $NaPO_3$) were dissolved in 25 cc of double distilled water. Both solutions were mixed at room temperature and stirred under ambient conditions until homogeneous. The stirred solution was left for 120 h. The resulting solution was neutralized to pH 7 by addition of alkali (0.1 N NaOH). The neutralized solution was stirred for 6 h under ambient conditions. Then it was left for 120 h. The resulting product was filtered, washed and dried in desiccators. Highly purified, deionized water was used in all solutions. Second distillation was carried out from alkaline $KMnO_4$ using an all-glass distillation apparatus.

Experimental procedures

An Infrared spectroscopy (IR) spectrum was obtained using a Thermo-Nicolet Avatar 370 of solid sample. Differential scanning calorimeter (DSC) measurements were performed on a Mettler Toledo, DSC 822 on 278 and 283 K min^{-1} under atmospheric oxygen. C–H–N–S analyser was performed on an Elementar systeme, vario EL III. The X-ray crystallography measurement of powder sample was carried out using Bruker AXS D8 Advance. Inductively coupled plasma-atomic emission spectrometer (ICP-AES) measurement was performed using Thermo Electron IRIS Intrepid II XSP DUO system for Ni, P and S determination as follows. The sample was dissolved in 5 mL HNO$_3$ and made up into 100 mL using HPLC grade water. IR, DSC, X-RD, ICP-AES and C–H–N–S analyses were performed at ST&IC, Cochin University of Science and Technology, Cochin. To determine the crystal structure of nickel compound X-ray diffraction, data are collected at room temperature with graphite-monochromated Mo Kα radiation on an XPERT PRO diffractometer operating in $\omega/2\theta$ scan mode. The pH measurements were performed using a Nucleonix type DP 301 digital pH meter equipped with combination of glass–Ag/AgCl/Cl^{-} (3 mol dm^{-3} NaCl) electrode. It was calibrated with standard buffers of pH 4.0, 7.0 and 9.0 (Merck).

Results and discussion

IR spectrometry

The P–H stretching frequency of the complex was 2360 cm^{-1} [41]. The broad band at 1652 cm^{-1} was due to crystal waters [42]. The peak 1397 cm^{-1} was due to S=O stretching frequency [43, 44]. The asymmetric stretching vibration of O–P–O was 1059 cm^{-1} [45]. The (P–O–P)$_{as}$ vibration of BOs in linkages was 888 cm^{-1} [46–48]. The Ni–O stretching vibration was 449 cm^{-1} [49].

Elemental analysis

C, H, N, S analysis

The elemental analysis of the bulk product was also consistence with the theoretical values. Anal. Calcd. for complex {Ni$_4$P$_4$SH$_{70}$Na$_x$O$_y$} is H 2.52%, S 1.15%; found H 2.53%, S 1.17%.

ICP-AES analysis

The elemental analysis of complex was carried out by ICP-AES. The Ni, P and S were also consistent with the

theoretical values. Anal. Calcd. for complex {$Ni_4P_4SH_{70}$-Na_xO_y} is S 1.15%, Ni 8.446%, P 4.453%; found S 1.15%, Ni 8.447%, P 4.378%.

X-ray crystallography

Crystal data and experimental details of the title compound are collected in Table 1. The X-RD spectrum of complex is shown in Fig. 1.

The H···H bond length was found at 1.319 Å and made an angle of 71.45°. These H atoms of water molecule were found in difference Fourier maps and refined with H···H bond length 1.32(2) Å. The S–O bond length of the compound is found 1.464 Å instead of 1.49–1.51 Å [50] and this plane was made at an angle of 63.46°. The terminal P–O bond length was 1.504 Å instead of average bond length 1.512 and 1.514 Å [51] and made an angle of 61.57°. The terminal P–O(–H) bond length was 1.571 Å

instead of 1.569(2) Å and made an angle of 58.71°. In this case P–O(–P) bond length was 1.608 Å instead of shortened bond length of 1.598(1) Å and made an angle of 57.22°. The distance P···O bond length was found 1.750 Å instead of 1.76 Å [52] and made an angle of 52.22°. The P–S bond length was 1.980 Å instead of 2.005 Å [53] and this plane made an angle of 45.77°. In the coordination sphere of Ni^{II}, the equatorial bond lengths of Ni–O was 2.025 Å instead of 2.036(2) Å [54] and made an angle of 44.70°. The axial bond length was 2.139 Å instead of 2.127(2) Å [55, 56] and this axial plane made an angle of 42.20°. Some nickel(II) made bond with phosphorous. The Ni–P bond length was 2.193 Å instead of 2.180(2) Å [57, 58] and this plane made an angle of 41.11°. The Ni–S bond length was found 2.286 Å instead of 2.24(3) Å [59] and this plane made an angle of 39.37°. The P–O–H bond length was 2.459 Å and made an angle of 36.50°. The Na–O bond length was 2.645 Å. The most probable d(Na–O) was 2.65 Å as per Angeli et al. [60] and this result was also consistent with average d(Na–O) from EXAFS data 2.63 Å as given by McKeown et al. [61]. This Na–O plane made an angle of 33.85°. The Ni–Ni bond distance was found to be 2.90 Å similar to Kriley et al. This was showing a lack of any Ni–Ni metal bonding. From this compound was shown to be an intermediate in the synthesis of the bridging phosphido nickel complex [62]. This plane made an angle of 30.71°. The P–O–P–O bond length was 3.148 Å and made an angle of 28.32°. The axial Ni–O–Na bond length was 4.772 Å and made an angle of 18.57°. The bond length of HO–S–Ni–O–P was 7.47 Å. In this plane Ni–O and P–O bonds were axial and terminal of the compound, respectively. This plane made an angle of 11.83°. In this plane the S–OH bond length was 1.549(3) Å [63]. The numerical values of this pattern are listed in Table 2.

Table 1 Crystal data and experimental details of the title compound

Empirical formula	$Ni_4P_4SH_{70}Na_xO_y$
Molecular mass/g	2782.6
Temperature/K	298
Wavelength/Å	1.542475
Crystal colour	Bluish
Theta range for data collection/°	3.0–80
Number of points	9500
Scan axis	Gonio
Scan step size	0.01
Time per step	0.2
Scan type	Continuous
$K\alpha_2/K\alpha_1$	0.5
$h\,k\,l$	0 0 0

Fig. 1 X-RD spectrum of complex
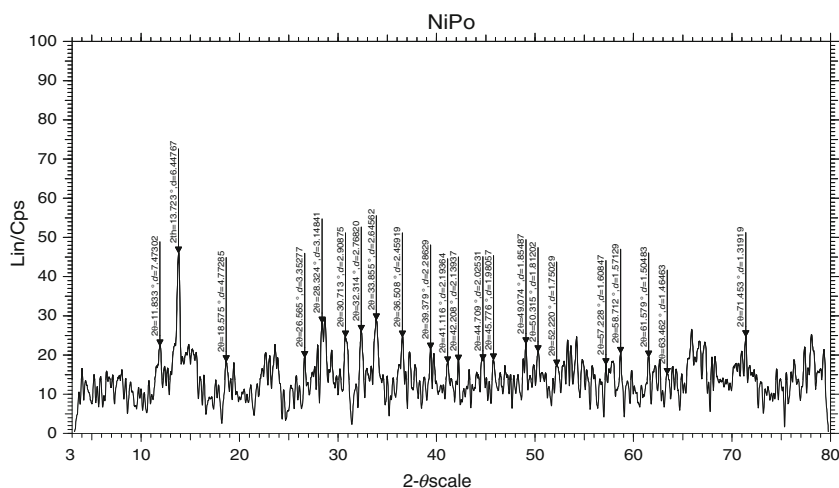
NiPo - File: SAIFXR091105A-02(NiPo).raw - Type: 2Th/Th locked - Start: 3.000 ° - End: 80.000 ° - Step: 0.010 ° - Step time: 0.2 s - Temp.: 25 °C (Room) - Time Started: 11 s - 2
Operations: Smooth 0.150 | Smooth 0.150 | Background 1.000,1.000 | Import

Table 2 X-ray powder diffraction numerical values and pattern of nickel compound

Peak no.	$2\theta/°$	d value/Å	I/I_0
1	11.83	7.473	50
2	13.72	6.447	100
3	18.57	4.772	41
4	26.56	3.352	41
5	28.32	3.148	63
6	30.71	2.908	58
7	32.31	2.768	58
8	33.85	2.645	63
9	36.50	2.459	58
10	39.37	2.286	50
11	41.11	2.193	41
12	42.20	2.139	41
13	44.70	2.025	41
14	45.77	1.980	39
15	49.07	1.854	52
16	50.31	1.812	43
17	52.22	1.750	36
18	57.22	1.608	36
19	58.71	1.571	43
20	61.57	1.504	41
21	63.46	1.464	30
22	71.45	1.319	54

Differential scanning calorimetry

From Eq. 1, one obtained by means of standard thermodynamic relations a specific heat [27]

$$C = k_B \beta^2 \frac{\partial}{\partial \beta^2} \ln(Z) \tag{2}$$

Here, k_B is the Boltzmann constant and the temperature T appears $\beta = 1/k_B T$. In the following, I assumed the removal particle to consist of harmonic oscillators and the coupling to be bilinear in complex and removal coordinates. In order to know the appearance of negative specific heat (2), it was sufficient to consider a stylized minimal model where the remove particle consisted of only a single degree of freedom described by the Hamiltonian.

$$H_R = \frac{P^2}{2m} + \frac{f_R}{2} q^2 \tag{3}$$

where f_R denotes the spring constant. The complex governed by the Hamiltonian

$$H_C = \frac{P^2}{2M} + \frac{f_c}{2} Q^2 \tag{4}$$

In the case of free particle, oxidation (O_2) (spring constant $f_c = 0$) and of a harmonic oscillator $(f_c > 0)$, the coupling Hamiltonian is given by

$$H_{CR} = -f_R qQ + \frac{f_R}{2} Q^2 \tag{5}$$

The mass of a single remove particle oscillator was m. This removal particle coupled with complex having mass M harmonically. In my analysis a free particle (O_2) was in contact with the single degree of freedom environment described by Eqs. 3 and 5. Complex and removal particles are assumed to stay in thermal equilibrium with each other at the inverse temperature β. Hence, the density matrix of the total system is given by a Gibb's state.

$$\rho_{CR} = Z_{CR}^{-1} \exp[-\beta(H_C + H_R + H_{CR})] \tag{6}$$

where $Z_{CR} = T_r \exp[-\beta(H_C + H_R + H_{CR})]$ denotes the partition function of the total system.

The partition function $Z_R = T_r \exp[-\beta H_R]$ of the removal particle's degree of freedom is given by

$$Z_R = \frac{1}{2 \sin\left(\frac{\hbar \beta \omega_0}{2}\right)} \tag{7}$$

where

$$\omega_0^2 = \left(\frac{f_R}{m}\right) \tag{8}$$

ω_0 was the frequency of remove particle oscillator. From Eq. 2 the specific heat capacity of this removal particles are given below.

$$C_R = k_B g\left(\frac{\hbar \beta \omega_0}{2}\right) \tag{9}$$

where

$$g(x) = \left(\frac{x}{\sin x}\right)^2$$

In order to obtain a well-defined partition function for the free particle, I restricted its motion to a region of inside the system. The system is supposed to be sufficiently large such that the energy level spacing can be neglected in compared with the thermal energy $k_B T$ [27]. Under this condition the space of this system will turn out to be irrelevant in the sequel.

The frequency of underdamped complex $(\varsigma < 1)$

$$\omega = \omega_0 \left\{ \varsigma \pm (\varsigma^2 - 1)^{\frac{1}{2}} \right\}$$

ς is called as damping ratio. In this case the complex loses energy along with removal particles and return to the thermally stable state.

The specific heat capacity of complex is given below

$$C_C = k_B g\left(\frac{\hbar\beta\omega}{2}\right).$$

The total heat capacity of the system is given below

$$C = C_C + C_R = -k_B g\left(\frac{\hbar\beta\omega}{2}\right) + k_B g\left(\frac{\hbar\beta\omega_0}{2}\right).$$

Heating rate 278 K min^{-1}

The damping ratio <1 on T < 592.2 K at 278 K min^{-1}, the specific heat capacity of the complex was negative. Hence, the specific heat capacity of the total system was negative.

At 278 K min^{-1}, at temperature ≥592.2 K the damping ratio was >1 and specific heat capacity was positive. The onset, peak and endset temperatures for two peaks were 305, 363 and 444 K for 1st peak and for 2nd peak 472, 494 and 500 K, respectively. The heat capacity for 1st and 2nd peak was −250.93 and −98.73 W g^{-1}, respectively. The heat capacity was positive after 592.2 K.

Heating rate 283 K min^{-1}

The damping ratio <1 at 283 K min^{-1}, the specific heat capacity of the complex was negative. Hence, the specific heat capacity of the total system was negative.

At 283 K min^{-1}, only one peak obtained. The onset, peak and endset temperatures for this peak were 304.5, 362.5 and 471 K, respectively. The heat capacity was −369.25 W g^{-1}.

The experimental molar heat capacities, enthalpy, entropy and specific heat factor are listed in Table S1. These are fitted in polynomial equation with temperature. The entropy is calculated from $C_P \ln T$.
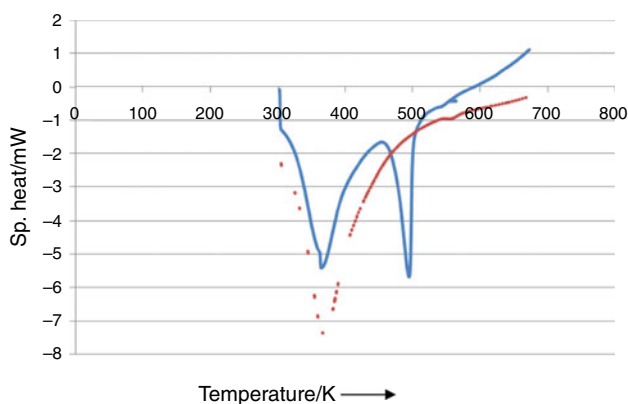

Fig. 2 DSC spectrum of complex at 278 K min^{-1} (*solid line*) from which negative specific heat was evaluated below temperature 592.2 K and above this temperature heat capacity was positive. The *dotted line* at 283 K min^{-1} from which negative specific heat was evaluated at all temperatures

The polynomial equation for specific heat capacity, enthalpy and entropy derived from DSC (Fig. 2) is given below

$$Y\{(C_P), (H_T - H_{303}), (S_T - S_{303})\}$$
$$= a_n T^n + a_{n-1} T^{n-1} + \cdots + a_2 T^2 + a_1 T + C.$$

The values of $a_1, a_2, a_3, \ldots, a_n$ and C are given in Table S1.

The complex is heated at atmospheric oxygen at heating rate of 278 and 283 K min^{-1}. The weight of complex should increase due to oxidation (addition of oxygen) but this increase in weight was less than that of weight loss due to high heating rate. So, the increase in weight is not detected during DSC measurements.

Conclusions

A new inorganically template metaphosphate of nickel(II) complex synthesized and characterized by different measurements is mainly of thermodynamical character. The specific heat capacity of complex was found negative at higher heating rates while at lower heating rate the specific heat capacity was found positive after 592.167 K at 278 K min^{-1} as damping ratio >1.

References

1. Cao G, Hong H, Mallouk TE. Layered metal phosphates and phosphonates: from crystals to monolayers. Acc Chem Res. 1992;25:420–7.
2. Feng S, Xu R. New materials in hydrothermal synthesis. Acc Chem Res. 2001;34:239–47.
3. Clearfield A, Sharma CVK, Zhang B. Crystal engineered supramolecular metal phosphonates: crown ethers and iminodiacetates. Chem Mater. 2001;13:3099–112.
4. Lohse DL, Sevov SC. Co$_2$(O$_3$P-CH$_2$-PO$_3$)·H$_2$O: a novel microporous diphosphonate with an inorganic framework and hydrocarbon-lined hydrophobic channels. Angew Chem Int Ed Engl. 1997;36:1619–21.
5. Serre C, Ferey G. Hydrothermal synthesis and structure determination from powder data of new three-dimensional titanium(IV) diphosphonates Ti(O$_3$P-(CH$_2$)n-PO$_3$) or MIL-25n (n = 2, 3). Inorg Chem. 2001;40:5350–3.
6. Soghomonian V, Chen Q, Haushalter RC, Zubieta J. Investigations into the targeted design of solids: hydrothermal synthesis and structures of one-, two-, and three-dimensional phases of the oxovanadium-organodiphosphonate system. Angew Chem Int Ed Engl. 1995;34:223–6.
7. Rodgers JA, Harrison WTA. Ethylenediamine zinc hydrogen phosphate, [H$_2$N(CH$_2$)$_2$NH$_2$]$_{0.5}$·ZnHPO$_3$, containing two independent, interpenetrating, mixed inorganic/organic networks. Chem Commun. 2000;2385–86.

8. Harrison WTA, Phillips MLF, Nenoff TM. $(CN_3H_6)_2 \cdot Zn(HPO_3)_2$: an open-framework zincophosphite built up from polyhedral 12-rings. Dalton Trans. 2001;2459–61.

9. Lin ZE, Zhang J, Zheng ST, Yang GY. Synthesis and characterization of a novel open-framework nickel-zinc phosphate with intersecting three-dimensional 16-ring channels. J Mater Chem. 2004;14:1652–5.

10. Gordon LE, Harrison WTA. Amino acid templating of inorganic networks: synthesis and structure of L-asparagine zinc phosphate, $C_4N_2O_3H_8 \cdot ZnHPO_3$. Inorg Chem. 2004;43:1808–9.

11. Fernandez S, Pizarro JL, Mesa JL, Lezama L, Arriortua MI, Olazcuaga R, Rojo T. Two new three-dimensional vanadium(III) and iron(III) phosphites template by ethylenediamine:$(C_2H_{10}N_2)_{0.5}$ $[M(HPO_3)_2]$. Ab initio structure determination, spectroscopic, and magnetic properties. Chem Mater. 2002;14:2300–7.

12. Fernandez S, Pizarro JL, Mesa JL, Lezama L, Arriortua MI, Rojo T. Hydrothermal synthesis of a new layered inorganic-organic hybrid cobalt(II)phosphite: $(C_2H_{10}N_2)[Co_3(HPO_3)_4]$: crystal structure and spectroscopic and magnetic properties. Int J Inorg Mater. 2001;3:331–6.

13. Fernandez S, Pizarro JL, Mesa JL, Lezama L, Arriortua MI, Rojo T. $(C_2H_{10}N_2)[Cr(HPO_3)F_3]$: the first organically template fluorochromium(III)phosphite. Angew Chem Int Ed Engl. 2002;41:3683–5.

14. Fernandez S, Pizarro JL, Mesa JL, Lezama L, Arriortua MI, Olazcuaga R, Rojo T. A new layered inorganic-organic hybrid manganese(II)phosphite: $(C_2H_{10}N_2)[Mn_3(HPO_3)_4]$. Hydrothermal synthesis, crystal structure, and spectroscopic and magnetic properties. Chem Mater. 2000;12:2092–8.

15. Zhang YN, Zhou BB, Li YG, Su ZH, Zhao ZF. A new molybdenum(V) nickel phosphate based on divacant $[H_{30}(Mo(V)_{16}O_{32})$ $Ni_{14}(PO_4)_{26}O_2(OH)_4(H_2O)_8]_{12}$- wheel. Dalton Trans. 2009;43:9446–51.

16. Wu H, Gao Y, Li H. Controlled synthesis of nickel phosphate hexahedronal and flower-like architectures via a simple template-free hydrothermal route. Cryst Eng Commun. 2010;12:3607–11.

17. Lin SC, Chen SY, Cheng S-Y, Lin JC. Synthesis and magnetic properties of highly arrayed nickel-phosphate nanotubes. Solid State Sci. 2005;7(7):896–900.

18. Samadi-Maybodi A, Nejad–Darzi SKH, Akhoondi R. Synthesis and characterization of nickel phosphate nanoparticles and VSB-5 with quaternary ammonium base. Int Nano Lett. 2011;1(1):52–8.

19. Jian D, Gao Q, Gao D, Ruan M, Shi W. Preparation of CdS semiconductor nanoarrays in the channels of nickel phosphate VSB-5 nanorods. Phys Lett A. 2006;357(2):136–40.

20. Guillou N, Gao Q, Forster PM, Chang JS, Park SE, Ferey G, Cheetham AK. Nickel(II) phosphate VSB-5: a magnetic nanoporous hydrogenation catalyst with 24-ring tunnels. Angew Chem Int Ed. 2001;40:2831–4.

21. Swain T. Synthesis, structural and thermal characterization of metaphosphatecobalt(II) salt. J Therm Anal Calorim. 2011;103:1111–7.

22. Swain T. Synthesis and thermal characterization of sulfur containing methionine bridged cobalt(III) and copper(II) complex. J Therm Anal Calorim. 2011. doi:10.1007/s10973-011-1751-y.

23. Lynden-Bell D, Wood R. The gravo-thermal catastrophe in isothermal spheres and the onset of red-giant structure for stellar systems. Mon Not R Astr Soc. 1968;138:495–525.

24. Hanggi P, Ingold G-L. Quantum Brownian motion and the third law of thermodynamics. Acta Phys Pol B. 2006;37:1537–50.

25. Horhammer C, Buttner H. Information and entropy in quantum Brownian motion thermodynamic entropy versus von Neumann entropy. J Stat Phys. 2008;133:1161–74.

26. Bandyopadhyay M. Quantum thermodynamics of a charged magneto-oscillator coupled to a heat bath. J Stat Mech Theory Exp. 2009. doi:10.1088/1742-5468/2009/05/P05002.

27. Hanggi P, Ingold G-L,Talkner P. Finite quantum dissipation: the challenge of obtaining specific heat. New J Phys. 2008. doi:10.1088/1367-2630/10/11/115008.

28. Wang C-Y, Bao J-D. The third law of quantum thermodynamics in the presence of anomalous couplings. Chin Phys Lett. 2008;25:429–32.

29. Kumar J, Sreeram PA, Dattagupta S. Low-temperature thermodynamics in the context of dissipative diamagnetism. Phys Rev E. 2009. doi:10.1103/PhysRevE.79.021130.

30. Ingold G-L, Hanggi P, Talkner P. Specific heat anomalies of open quantum systems. 2009. doi:10.1103/PhysRevE.79.061105.

31. Wiesniak M, Vedral V, Brukner C. Heat capacity as an indicator of entanglement. Phys Rev B. 2008. doi:10.1103/PhysRevB.78.064108.

32. Caldena AO, Leggett AJ. Quantum tunnelling in a dissipative system. Ann Phys (N.Y.). 1983;149:374–456.

33. Grabert H, Weiss U, Talkner P. Quantum theory of the damped harmonic oscillator. Z Phys B. 1984;55(1):87–94.

34. Leggett AJ, Chakravarty S, Dorsey AT, Fisher MPA, Garg A, Zwerger W. Dynamics of the dissipative two-state system. Rev Mod Phys. 1987;59:1–85.

35. Grabert H, Schramm P, Ingold G-L. Quantum Brownian motion: the functional integral approach. Phys Rep. 1988;168(3):115–207.

36. Ford GW, Lewis JT, Connell RFO. Quantum oscillator in a blackbody radiation field II. Direct calculation of the energy using the fluctuation-dissipation theorem. Ann Phys (N.Y.). 1988;185(2):270–83.

37. Hanke A, Zwerger W. Density of states of a damped quantum oscillator. Phys Rev E. 1995;52(6):6875–8.

38. Dittrich T, Hanggi P, Ingold G-L, Kramer B, Schon G, Zwerger W. Quantum transport and dissipation. Chap. 4. New York: Wiley; 1998.

39. Ford GW, Connell RFO. Quantum thermodynamic functions for an oscillator coupled to a heat bath. Phys Rev B. 2007. doi:10.1103/PhysRevB75.134301.

40. Ingold G-L. Path integrals and their application to dissipative quantum systems. Lect Notes Phys. 2002;611:1–53.

41. Yang Y, Zhao Y, Yu J, Zhou Y, Pang N, Su H, Pang S. Template syntheses of two open-framework zinc phosphites. Zeitschrift fur anorganische und allgemeire Chemie. 2008;634(10):1780–4.

42. Nakamoto K. Infrared and Raman spectra of inorganic and coordination compounds, part A: theory and applications in inorganic chemistry. 5th ed. New York: Wiley; 1997.

43. Saur O, Bensitel M, Saad ABH, Lavalley JC, Tripp CP, Morrow BA. The structure and stability of sulfated alumina and titania. J Catal. 1986;99:104–10.

44. Morrow BA, McFarlane RA, Lion M, Lavalley JC. An infrared study of sulfated silica. J Catal. 1987;107(1):232–9.

45. Zhang D, Yue H, Shi Z, Feng S. Hydrothermal synthesis and structural characterization of organically templated zincophosphites: $[C_6H_{22}N_4]_{0.5}[Zn_2(HPO_3)_3]$ and $[C_3N_2H_5]$ $[Zn_{1.5}(HPO_3)_2]$. Solid State Sci. 2005;7(10):1256–60.

46. Abid M, Sabiron M, Taibi M. Structure and DC conductivity of lead sodium ultraphosphate glasses. Mater Sci Eng B. 2003;97(1):20–4.

47. Byun JO, Kim BH, Hong KS, Jung HJ, Lee SW, Izyneev AA. Properties and structure of $RO–Na_2O–Al_2O_3–P_2O_5$ (R = Mg, Ca, Sr, Ba) glasses. J Non-Cryst Solids. 1995;190(3):288–95.

48. Liu HS, Chin TS, Yung SW. FTIR and XPS studies of low-melting $PbO-ZnO-P_2O_2$ glasses. Mater Chem Phys. 1997;50(1):1–10.

49. Gaballa AS, Telab SM, Nour EM. Preparation, spectroscopic and thermal studies of the bridged isocyanato complex $[NI_2(NCO)_2$ $(H_2O)_4]X_2$, (X = ½SO_4^{2-} OR NO_3^-). J Argent Chem Soc. 2005;93(4–6):233–9.

50. Remko M, Swart M, Bickelhaupt FM. Conformational behavior of basic monomeric building units of glycosaminoglycans:

isolated systems and solvent effect. J Phys Chem B. 2007;
111(9):2313–21.

51. Leung KY, Calvo C. The structure of Na$_4$P$_2$O$_7$ at 22 °C. Can J
Chem. 1972;50(16):2519–26.

52. Kavounis CA, Bozopoulos AP, Cheer CJ. A phosphorous ylide
with a secondary P⋯O bond. The crystal structure of a-[6-fu-
razano][3,4-b]-quinoxalinyl-a-carbethoxymethylene triphenyl-
phosphorane(butene-2,3,4-dimethylhexene-3)solvate. Zeitschrift
fur Kristallographie. 1989;188(3–4):299–306.

53. Saglam EG, Celik O, Ide S, Yilmaz H. Synthesis and determi-
nation of crystal and molecular structure of {bispyridine-bis[4-
methoxyphenyl(3-methylbutyl) dithiophosphinato]}nickel(II).
X-Ray Struct Anal Online. 2011;27(5):23–4.

54. Okabe N, Muranishi Y. Cobalt(II) and nickel(II) complexes of
isoquinoline-1-carboxylate. Acta Crystallogr C. 2002;58(12):
m578–80.

55. Yang M-X, Lin S, Yu P, Chen L-J, Liu S-X. Syntheses, structures
and antibacterial activities of two nickel(II) complexes with
N-hexanoylsalicylhydrazide ligand. Chin J Chem. 2005;23(10):
1407–11.

56. Lu T-B, Xiang H, Luck RL, Mao Z-W, Chen X-M, Ji L-N.
Molecular architecture via coordination and multi-intermolecular
interactions: synthesis, structures and magnetic properties of one-
dimensional coordination polymers of macrocyclic nickel(II)
complexes with terephthalate and trans-butene dicarboxylate.
Inorg Chem Acta. 2003;355:229–41.

57. Milbrath DS, Springer JP, Clardy JC, Verkade JG. Crystal and
molecular structure of bromotetrakis(trimethyl phosphi-
to)nickel(II) tetrafluoroborate, {Ni[P(OCH$_3$)$_3$]$_4$Br}BF$_4$. Inorg
Chem. 1975;14(11):2665–8.

58. Cao R, Huang Z-Y, Lei X-J, Kang B-S, Hong M-C, Liu H-Q.
Synthetic and structural chemistry of nickel(II) complexes con-
taining dithiolato and phosphine ligands. 1. Preparation and
crystal structure of Ni$_2$(PPh3)$_2$(edt)$_2$. Chin J Chem. 1992;10(3):
227–31.

59. Kodama K, Fujishita H, Harashina H, Taniguchi S, Takeda J,
Sato M. Structural studies on the quasi two-dimensional Mott
system BaCo$_{1-x}$Ni$_x$S$_{2-\delta}$ by the X-ray Rietveld method. J Phys Soc
Jpn. 1995;64(6):2069–73.

60. Angeli F, Delaye JM, Charpentier T, Petit JC, Ghaleb D, Faucon
P. Influence of glass chemical composition on the Na–O bond
distance: a ^{23}Na 3Q-MAS NMR and molecular dynamics study.
J Non-Cryst Solids. 2000;276:132–44.

61. McKeown DA, Waychunas GA, Brown GE. Exafs and xanes
study of the local coordination environment of sodium in a series
of silica-rich glasses and selected minerals within the Na$_2$O–
Al$_2$O$_3$–SiO$_2$ system. J Non-Cryst Solids. 1985;74(2–3):325–48.

62. Kriley CE, Woolley CJ, Krepps MK, Popa EM, Fanwick PE,
Rothwell IP. Synthesis and characterization of a series of novel
nickel(II)/nickel(I) complexes. Crystal structures of [NiCl$_2$
(dcpm)], [Ni(dcpm)$_2$](NO$_3$)$_2$·2EtOH, [Ni$_2$Cl$_2$(μ-dcpm)$_2$(μ-H)]
and [Ni$_2$(μ-PCy$_2$)$_2$(PCy$_2$Me)$_2$]; dcpm = bis(dicyclohexylphos-
phino)methane. Inorg Chim Acta. 2000;300–302:200–5.

63. McCabe PH, Milne NJ, Sim GA. Structure of the hydrogensulfate
salt of a diazaadamantanone, 5,7-diphenyl-1,3-diazatricyclo[3.3.1.
13, 7]decane-6-one. Acta Crystallogr C. 1989;45(1):114–6.